Solid State Sciences 147 (2024) 107361

Contents lists available at ScienceDirect

Solid State Sciences

journal homepage: www.elsevier.com/locate/ssscie

AGe_2O_4Q (A = Ba, Sr; Q = S, Se): A series of heteroanionic oxychalcogenides with large birefringence

Dong Gao [a,1], Fuqiang Chen [a,1], Hongping Wu [a], Zhanggui Hu [a], Jiyang Wang [a], Yicheng Wu [a], Hongwei Yu [a,**], P Shiv Halasyamani [b,*]

[a] Tianjin Key Laboratory of Functional Crystal Materials, Institute of Functional Crystal, Tianjin University of Technology, Tianjin, 300384, China
[b] Department of Chemistry, University of Houston, 112 Fleming Building, Houston, TX, 77204-5003, United States

ARTICLE INFO

Keywords:
Oxychalcogenides
Heteroanions
Birefringence
Crystal structures

ABSTRACT

Heteroanionic materials are of current research interest owing to their varied structural chemistry and properties. Recently, a number of heteroanionic materials have been synthesized that can be used for water splitting, battery materials, thermoelectrics, and nonlinear optical applications. Birefringent heteroanionic materials are still rarely researched. Herein, we report a series of new oxychalcogenides, AGe_2O_4Q (A = Ba, Sr; Q = S, Se), that are synthesized by solid-state reactions in fused silica tubes with their structures determined by single-crystal X-ray diffraction. Optical property measurements show that AGe_2O_4Q (A = Ba, Sr; Q = S, Se) exhibit large birefringences, 0.13–0.19 @ 1064 nm. These are one-order of magnitude larger than their single-anionic homologue, $BaGe_2O_5$ - 0.03 @ 1064 nm. This suggests that constructing heteroanions through using chalcogenides to partially substitute O in tetrahedral foundation building units (FBUs) is a viable method for designing new birefringent materials. Furthermore, the crystal structures, UV–vis–NIR diffuse reflectance spectra, infrared and Raman spectra as well as the first-principles calculations for AGe_2O_4Q (A = Ba, Sr; Q = S, Se) are also reported.

1. Introduction

Birefringence originates from the optical anisotropy of materials and plays indispensable important role for the development of advanced technology [1–6]. During the past decades, a number of the oxide-based birefringent crystals, such as YVO_4 [7], TiO_2 [8], $LiNbO_3$ [9] and $CaCO_3$ [10], have been discovered and commercialized in ultraviolet (UV) and visible regions. Recently, some borates with large birefringence and short UV cut-off edges ($\lambda_{cut\text{-}off}$ < 200 nm), such as $Na_3Ba_2(B_3O_6)_2F$ (0.113@589 nm) [11], $Ba_2Ca(B_3O_6)_2$ (0.124@589 nm) [12], $Ba_2Mg(B_3O_6)_2$ (0.110@589 nm) [13], $MBaYB_6O_{12}$ (M = Rb, Cs) (0.120@589 nm) [14], and $Ca(BO_2)_2$ (0.134@589 nm) [15] have also been reported. These materials may be potential deep-UV birefringent crystals. However, compared with UV, deep-UV and visible regions, the birefringent crystals in the infrared (IR) regions are rarely reported.

For design of the IR birefringent crystals, chalcogenides may be a good materials class because they can exhibit excellent transmission in wide IR regions [16,17]. Typically, sulfides are transparent to ~11 μm, selenides to ~15 μm, and tellurides to beyond 20 μm [18–20]. But for chalcogenide crystals, they generally possess narrow band-gaps, which are unfavorable for materials to exhibit high laser damage thresholds (LDT). That will limit their applications in the high-energy laser systems that are important for environmental monitoring and information communication [21–23]. In recent research, it has been shown that heteroanionic compounds can exhibit superior functional properties than the single-anionic compounds because the former can integrate the properties of the different anion groups [24,25]. Especially in the oxychalcogenides, many interesting functional materials have been found, such as the excellent thermoelectric materials, *e.g.* BiCuSeO [26], high-capacity battery cathode material, *e.g.* $Ag_2V_2O_6F_2$ [27], and the excellent nonlinear optical crystal, *e.g.* $Sr_6Ge_3OSe_{11}$ [28].

In the reported research, we believe that the heteroanionic oxychalcogenides will be interesting for the design of IR birefringent crystals. Firstly, the intrinsic difference between M-O and M-Q bonds in the heteroanionic $[MO_xQ_y]$ (Q = S, Se) groups is helpful for enhancing optical anisotropy of materials which can make materials to produce a

* Corresponding author.
** Corresponding author.
E-mail addresses: yuhw@email.tjut.edu.cn (H. Yu), psh@uh.edu (P.S. Halasyamani).
[1] These authors contributed equally to this work.

https://doi.org/10.1016/j.solidstatesciences.2023.107361
Received 26 September 2023; Received in revised form 26 October 2023; Accepted 31 October 2023
Available online 28 November 2023
1293-2558/

large birefringence. Secondly, in heteroanionic [MO_xQ_y] (Q = S, Se) groups, the M-Q bonds are helpful to reduce the IR absorptions of materials so that the materials can exhibit wide IR transmission regions [29–32]. Our research in the heteroanionic A-Ge-O-Q (A = alkaline earth; Q = S, Se) system have resulted in the discovery of four new heteroanionic oxychalcogenides, AGe_2O_4Q (A = Ba, Sr; Q = S, Se). They all exhibit large birefringence at 1064 nm, 0.13, 0.16, 0.15, 0.19 for $BaGe_2O_4S$, $BaGe_2O_4Se$, $SrGe_2O_4S$ and $SrGe_2O_4Se$, respectively. These birefringences are one-order magnitude larger than the one of their corresponding single-anionic homologue, $BaGe_2O_5$ (0.03 at 1064 nm) [33], indicating the effectiveness of heteroanionic groups for the design of the birefringent crystals. In addition, UV-VIS-NIR diffusion spectra and IR spectra also show these compounds also have wide band-gaps and wide IR transmission regions. Therefore, AGe_2O_4Q (A = Ba, Sr; Q = S, Se) may be potentials as IR birefringent crystals. Herein, we will report their syntheses, crystal structures, optical properties and the first principle calculations.

2. Experimental section

2.1. Reagents

BaF_2 (Aladdin Chemistry Co., Ltd., 99.9 %), Ba (Beijing Hawk Science and Technology Co. Ltd. 99.9 %), GeO_2 (Aladdin Chemistry Co., Ltd., 99.5 %), Ge (Beijing Hawk Science and Technology Co. Ltd. 98 %), SrS (Beijing Hawk Science and Technology Co. Ltd. 98 %), SrSe (Beijing Hawk Science and Technology Co. Ltd. 98 %), S (Aladdin Chemistry Co., Ltd., 99.5 %), and Se (Aladdin Chemistry Co., Ltd., 99.9 %) were used as received from commercial sources without any further purification.

2.2. Synthesis

AGe_2O_4Q (A = Ba, Sr; Q = S, Se) were all synthesized by the solid-state reactions in the fused silica tube. For $BaGe_2O_4S$(Se), the starting materials of BaF_2 (0.67 mmol, 0.1175 g), Ba (0.67 mmol, 0.0920 g), GeO_2 (1.00 mmol, 0.1046 g), Ge (0.33 mmol, 0.0240 g), and S/Se (1.33 mmol, 0.0426/0.1050 g) were used. For $SrGe_2O_4S$(Se), stoichiometric mixture of starting materials SrS/SrSe (1.00 mmol, 0.1197/0.1666 g) and GeO_2 (2.00 mmol, 0.2093 g) were used. These starting materials were put into graphite crucibles and were flame-sealed into 10 mm (inner diameter) fused-silica tubes under vacuum (~10^{-3} Pa), respectively. These tubes were then placed into a temperature controlled muffle furnace, heated from room temperature to 1123 K for $BaGe_2O_4S$ (Se) (1198 K for $SrGe_2O_4S$(Se)) in 40 h, kept at these temperatures for 96 h, and then cooled to room temperature at 2.5 °C/h. Colourless crystals of Ba(Sr)Ge_2O_4S (~45 % yield based on GeO_2) and light yellow crystals of Ba(Sr)Ge_2O_4Se (~40 % yield based on GeO_2)were obtained (Fig. S1).

2.3. Single-crystal structure determination

High-quality block single crystals of AGe_2O_4Q (A = Ba, Sr; Q = S, Se) were selected for single-crystal X-ray diffraction (XRD). Diffraction data were collected by using Mo $K\alpha$ radiation (λ = 0.71073 Å) on a Bruker SMART APEX II diffractometer equipped with a 4K CCD detector at room temperature [34]. Their structures were solved by direct methods and refined by full-matrix least-squares method on F^2 with anisotropic thermal parameters for all atoms using SHELXTL program package [35]. Besides, the PLATON program was used to check the symmetry, and no other missed or higher symmetry element was found [36]. Crystal data and structure refinement information were showed in Table 1. The atomic coordinates, equivalent isotropic displacement parameters and selected interatomic distances and angles of AGe_2O_4Q (A = Ba, Sr; Q = S, Se) were listed in Table S1 and Table S2 in the Supporting Information, respectively.

Table 1
Crystal data and structure refinement for AGe_2O_4Q (A = Ba, Sr; Q = S, Se).

Empirical formula	$BaGe_2O_4S$	$BaGe_2O_4Se$	$SrGe_2O_4S$	$SrGe_2O_4Se$
Formula weight	378.58	425.48	328.86	375.76
Space group	$P2_1/c$			
a (Å)	a = 6.9990 (12)	a = 7.179(7)	a = 6.6983 (11)	a = 6.7928 (6)
b (Å) β(°)	b = 9.4705 (18) β = 94.6110 (6)	b = 9.592(9) β = 96.160 (3)	b = 9.4824 (14) β = 94.355 (5)	b = 9.5694 (8), β = 95.357 (5)
c (Å)	c = 8.2181 (14)	c = 8.491(8)	c = 8.1342 (13)	c = 8.2785 (9)
Volume(Å^3)	542.97(17)	581.3(10)	515.16(14)	535.78(13)
Z	4			
ρ_{Calcd} (g/cm^3)	4.631	4.862	4.240	4.662
Completeness	99.90 %	99.30 %	99.60 %	100.0 %
Data/ parameters	1254/73	1336/73	1185/73	1233/74
Goodness-of-fit on F^2	1.091	1.070	1.046	1.051
Final R indexes [F_o^2>2s(F_o^2)][a]	R_1 = 0.0425, wR_2 = 0.1005	R_1 = 0.0574, wR_2 = 0.1552	R_1 = 0.0279, wR_2 = 0.0545	R_1 = 0.0225, wR_2 = 0.0376
Largest diff. peak and hole (e.Å^{-3})	1.778 and −3.604	2.001 and −4.555	0.818 and −0.787	0.669 and −0.634

[a] $R_1 = \sum||F_o| - |F_c||/\sum |F_o|$, $wR_2 = \{\sum[w(F_o^2 - F_c^2)^2]/\sum [w(F_o^2)^2]\}^{1/2}$.

2.4. Powder X-ray diffraction

Powder X-ray diffraction (PXRD) of AGe_2O_4Q (A = Ba, Sr; Q = S, Se) compounds were measured on the SmartLab9KW X-ray diffractometer analyzer with Cu-Kα radiation (λ = 1.5418 Å) in reflection mode at room temperature with a step size of 0.02° in the range of 2θ = 10−70°. The measured PXRD patterns exhibit a good consistency with the simulated ones except for a small amount of BaSe was detected in $BaGe_2O_4Se$ (Fig. 1).

2.5. UV–vis-IR diffuse reflectance spectroscopy and IR spectroscopy

Optical diffuse reflectance spectra were performed at room temperature with A Shimadzu SolidSpec-3700DUV spectrophotometer. Data were collected in the wavelength range 200–2400 nm. The IR spectra were recorded at room temperature by a Nicolet iS50 FT-IR spectrometer transform IR spectrometer in the 400–4000 cm^{-1} range. Polycrystalline powder of AGe_2O_4Q (A = Ba, Sr; Q = S, Se) were directly put on the test platform to obtain IR spectral vibration peaks.

2.6. Raman spectroscopy

The Raman spectra were collected with small bulk crystals on a confocal microscope-laser Raman spectrometer (WITec) equipped with a CCD detector using 532 nm radiation from a diode laser. Crystals were selected and loaded on a SiO_2 slide; then, a 50× objective lens was used to choose the area to be measured on the crystal. The spectrum data was collected using an integration time of 10 s.

2.7. Birefringence measurement

The birefringence of AGe_2O_4Q (A = Ba, Sr; Q = S, Se) were measured by using a cross-polarizing microscope. According to the equation $R = \Delta n \times d$, Δn can be obtained, where R, Δn, and d are retardation, birefringence, and thickness, respectively.

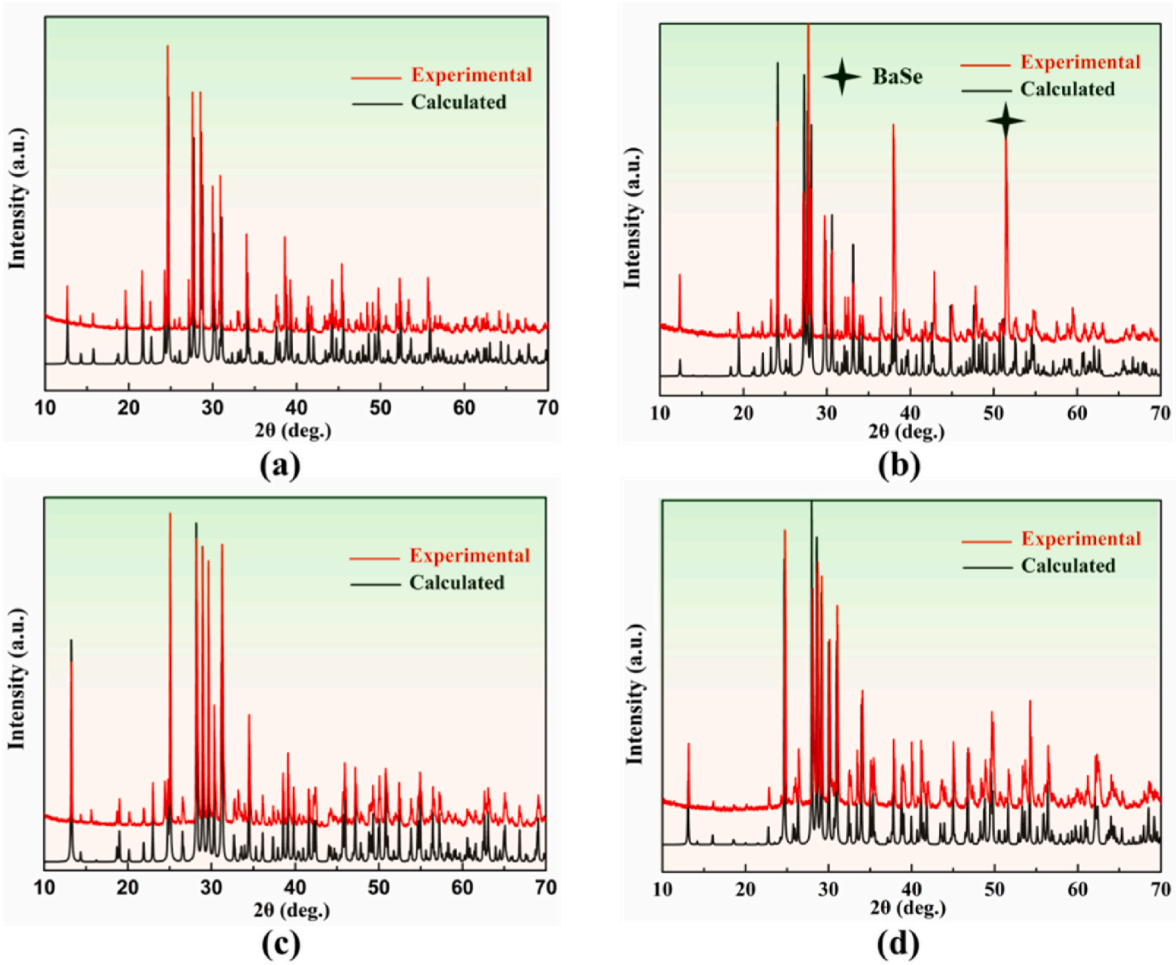

Fig. 1. Powder XRD of (a) $BaGe_2O_4S$, (b) $BaGe_2O_4Se$, (c) $SrGe_2O_4S$, and (d) $SrGe_2O_4Se$.

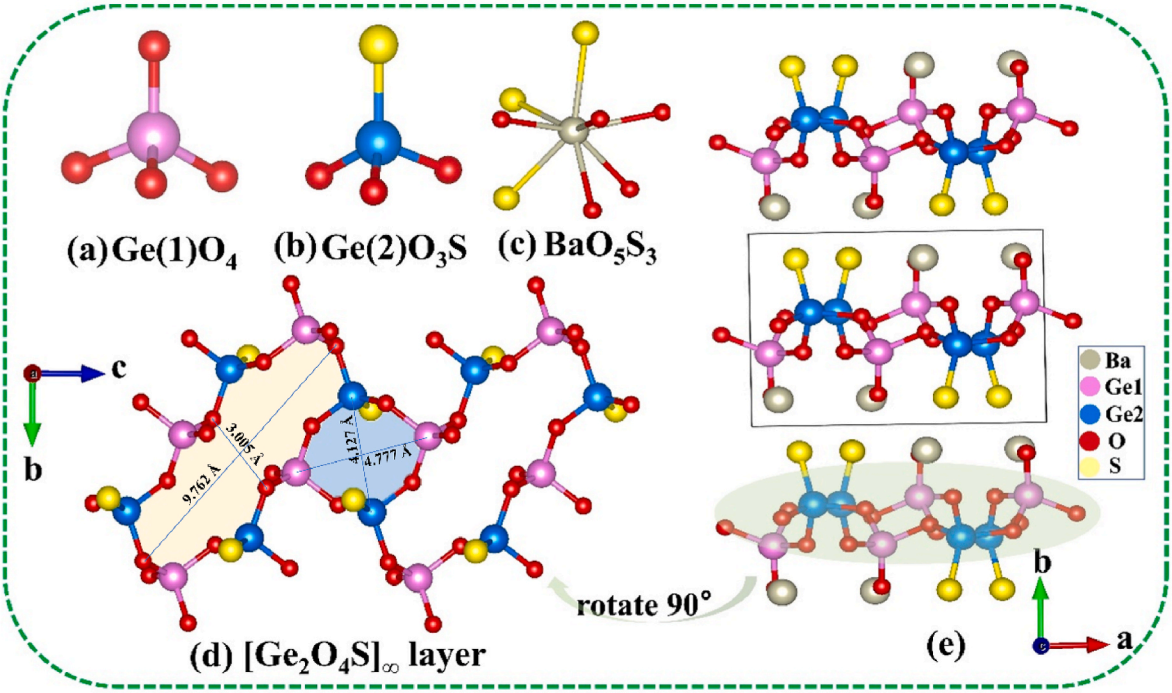

Fig. 2. The structure of $BaGe_2O_4S$: (a) $[Ge(1)O_4]$ unit; (b) $[Ge(2)O_3S]$ unit; (c) $[BaO_5S_3]$ unit; (d) 2D $[Ge_2O_4S]_\infty$ layered structure formed by the 16-membered rings and 8-membered rings; (e) the arrangement of 2D layered structures of anion units along *b*-direction.

2.8. Theoretical calculations

First-principles calculations of AGe_2O_4Q (A = Ba, Sr; Q = S, Se) were performed by a plane-wave pseudopotential density functional theory (DFT) method implemented on CASTEP software [37,38]. For embodying correlation, core−electron interactions were characterized by norm-conserving pseudopotentials (NCP) [39]. Meanwhile, the generalized gradient approximation (GGA) of Perdew-Buker-Ernzerhof (PBE) was exerted [40]. The valence states are as follows: Ba $5p^6 6s^2$, Sr $4p^6 5s^2$, Ge $4s^2 4p^2$, S $3s^2 3p^4$, Se $4s^2 4p^4$, and O $2s^2 2p^4$. To achieve energy convergence, the plane-wave energy cutoff was set at 810 eV for AGe_2O_4Q (A = Ba, Sr; Q = S, Se). The Brillouin zone involved 5 × 4 × 4 for AGe_2O_4S (A = Ba, Sr), and 5 × 3 × 4 for AGe_2O_4Se (A = Ba, Sr).

3. Results and discussion

3.1. Crystal structures

AGe_2O_4Q (A = Ba, Sr; Q = S, Se) crystallize in monoclinic space group $P2_1/c$. As AGe_2O_4Q (A = Ba, Sr; Q = S, Se), are iso-structural, only $BaGe_2O_4S$ is illustrated in detail as a representative. The asymmetric unit of $BaGe_2O_4S$ contains one Ba atom, two Ge atoms, four O atoms and one S atom, which all occupy the Wyckoff positions of 4*e*. For Ge atoms, they are all coordinated by O or O/S atoms to form tetrahedral single-anionic $[GeO_4]$ and heteroanionic $[GeO_3S]$ units (Fig. 2a and b), with the Ge–O bond distances ranging from 1.683(9) to 1.794(8) Å, and Ge–S bond distance is 2.103(4) Å. All of these Ge–O or Ge–S bonds have the consistent distances with the ones in other germinates or Ge-containing sulfides [41,42]. In the structure, the $[GeO_4]$ and $[GeO_3S]$ tetrahedra alternatively connect with each other to form the 16-membered rings and 8-membered rings, and then these 16-membered rings and 8-membered rings are further linked to form the two-dimensional (2D) $[Ge_2O_4S]_\infty$ layers by sharing O atoms (Fig. 2d). In connectivity terms, the structure may be written as $\{[Ge(1)O_{3/2}O_{1/1}][Ge(2)O_{3/2}S_{1/1}]\}^{2-}$ with Ba^{2+} cations filled between adjacent two layers to maintain the charges balanced (Fig. 2c, e). Remarkably, $Ge(2)O_3S$ and $Ge(1)O_4$ are staggered and antiparallel arranged with each other in the same layers, which cancels the macro-polarity and results in their centrosymmetric structures. The bond valence sum (BVS) calculations for Ba: 1.92; Ge: 4.20−4.25; S: 2.02 and O: 1.93−2.18 are agreement with their normal oxidation states, assuring the consistency of the crystal structures [43].

3.2. Structural comparison

From the viewpoint of structure, the heteroanionic $BaGe_2O_4S$ can be seen as the derivative of $BaGe_2O_5$ with one O atom is substituted by S atom (Fig. 3). But remarkably, $BaGe_2O_5$ and $BaGe_2O_4S$ are not iso-structural. $BaGe_2O_5$ features a 2D $[Ge_2O_5]_\infty$ layer that is composed of the $[GeO_4]$ and $[GeO_6]$ octahedra (Fig. 3a, c). For $BaGe_2O_4S$, although it also features a 2D $[Ge_2O_4S]_\infty$ layer, the layer is constructed of the tetrahedral $[GeO_4]$ and $[GeO_3S]$ units (Fig. 3d, f). That is, from $BaGe_2O_5$ to $BaGe_2O_4S$, the $[GeO_6]$ octahedra change to the $[GeO_3S]$ tetrahedra. The structural transformation can be understood based on the difference of ionic radius of O and S atoms and the valence matching principle [44]. In $BaGe_2O_5$, all Ba^{2+} cations are only coordinated by the O^{2-} anions. Because of the large difference of ionic radius of Ba^{2+} and O^{2-} anions, Ba^{2+} cations tend to be coordinated by more O^{2-} anions (twelve O^{2-} ions in $BaGe_2O_5$) (Fig. 3b). That makes Ba^{2+} cations have the low Lewis acid strength (2/12 = 0.17). As such, the coordinated O atoms of Ba^{2+} cations should be the bridged O atoms between GeO_4 and GeO_6 units because these bridged O atoms will have little residual negative charges and low Lewis base strengths. In addition, these bridged O atoms cannot be the bridged O atoms between GeO_4 and GeO_6 units because these bridged O atoms will have no more residual negative charges (Fig. 3g). In $BaGe_2O_5$, two different coordination environments of Ge atoms, the $[GeO_4]$ tetrahedra and the $[GeO_6]$ octahedra, are

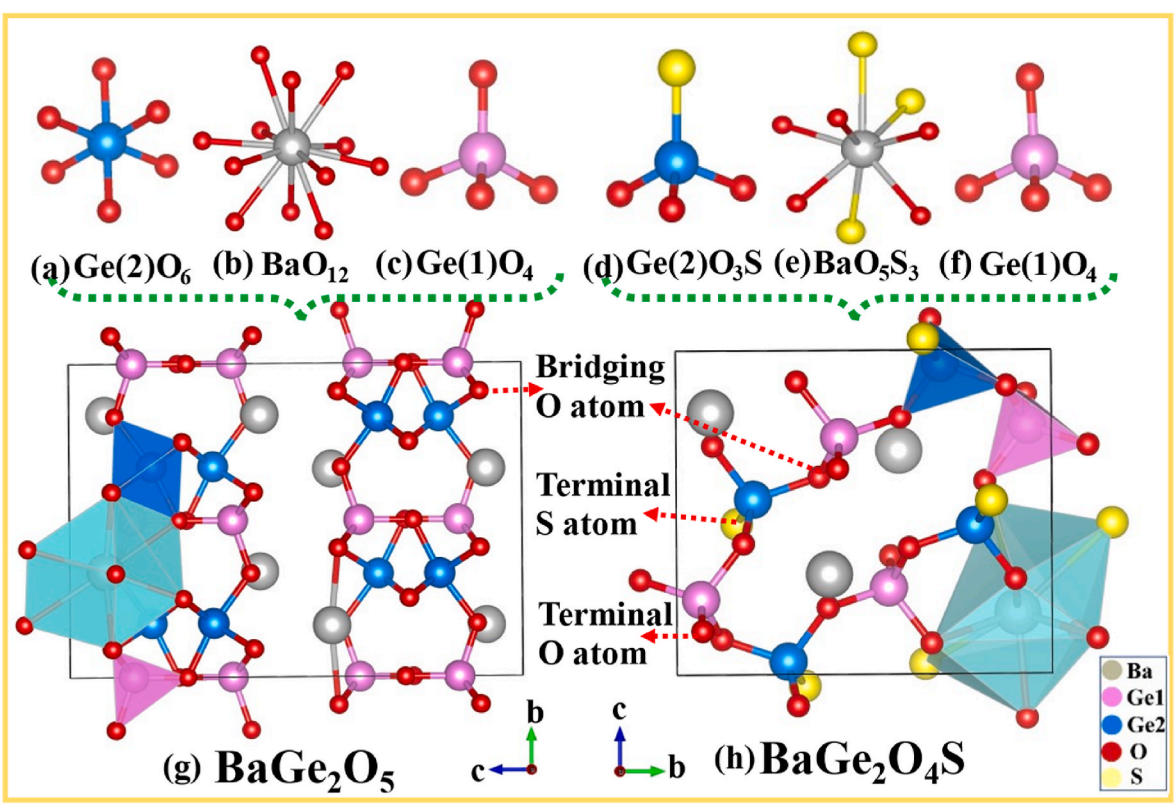

Fig. 3. (a) $Ge(2)O_6$ unit of $BaGe_2O_5$; (b) BaO_{12} unit of $BaGe_2O_5$; (c) $Ge(1)O_4$ unit of $BaGe_2O_5$; (d) $Ge(2)O_3S$ unit of $BaGe_2O_4S$; (e) BaO_5S_3 unit of $BaGe_2O_4S$; (f) $Ge(1)O_4$ unit of $BaGe_2O_4S$; (g) the structure of $BaGe_2O_5$; (h) the structure of $BaGe_2O_4S$.

observed. In $BaGe_2O_4S$, however, S^{2-} anions have closer ionic radius with Ba^{2+} cations. So, the coordination numbers of Ba^{2+} cations is less (eight in $BaGe_2O_4S$) and hence the Ba^{2+} cations have the relatively higher Lewis acid strength (2/8 = 0.25) (Fig. 3e). Thus, the coordinated O/S atoms of Ba^{2+} cations can be the terminal O/S atoms. But as the Lewis acid strength of Ba^{2+} cations is not high enough, the corresponding Ge–O/S bonds for the terminal O/S ions are shorten so that they have the relatively little negative charges left to match the Lewis acid strength of Ba^{2+} cations (Table S2). So, the basic building units (BBUs) in $BaGe_2O_4S$ must be tetrahedral $[GeO_4]$ and the $[GeO_3S]$ units (Fig. 3h). But the $[GeO_6]$ octahedra are impossible for $BaGe_2O_4S$ because the residual negative charges of terminal O atoms for octahedral $[GeO_6]$ would be too high, which cannot match with the Lewis acid strength of Ba^{2+} cations. Based on the above discussion, we can see that the heteroanionic $BaGe_2O_4S$ can exhibit larger structural anisotropy because of the intrinsic differences between Ge–O and Ge–S as well as the shorter terminal Ge–O/S distances (perpendicular to $[Ge_2O_4S]_\infty$ layer) than the bridged Ge–O distances (in the $[Ge_2O_4S]_\infty$ layer). The large structural anisotropy may be helpful to generate a large birefringence.

3.3. Birefringence measurements

The birefringence of AGe_2O_4Q (A = Ba, Sr; Q = S, Se) was measured by a cross-polarizing microscope in the visible region. The observed interference colors in cross-polarized light were second-order blue for $BaGe_2O_4S$ and $SrGe_2O_4S$. And, the interference color observed is second-order green under cross-polarized for $BaGe_2O_4Se$ and $SrGe_2O_4Se$ (Fig. 4). Matching with the Michal–Levy chart, the retardations (R values) were found to be 790 nm for second-order blue and 810 nm for second-order green. And their crystal thicknesses were found to be 9.3, 6.0, 9.5 and 6.8 μm, respectively. Following the equation $R = \Delta n \times d$, we can obtain that the birefringence of $BaGe_2O_4S$, $BaGe_2O_4Se$, $SrGe_2O_4S$ and $SrGe_2O_4Se$ are 0.09, 0.14, 0.08 and 0.12 in the visible region. Remarkably, as the cross-polarizing microscope can only measure the birefringence in the crystal wafers, the measured value may be smaller than the largest birefringence of materials. That means the birefringence of AGe_2O_4Q (A = Ba, Sr; Q = S, Se) may be larger than the measured values. The large birefringence might be favorable for their potential application as birefringent crystals.

3.4. UV–vis–NIR diffuse reflectance spectroscopy and IR spectroscopy

Furthermore, the optical band-gaps of AGe_2O_4Q (A = Ba, Sr; Q = S, Se) were also measured by the UV–vis–NIR diffuse reflectance spectra and they were converted into the absorption based on Kubelka–Munk Equation: $F(R) = K/S = (1-R)^2/2R$ [45]. As shown in Fig. 5, the optical band gaps of AGe_2O_4Q (A = Ba, Sr; Q = S, Se) are 4.32 eV, 3.68 eV, 4.20

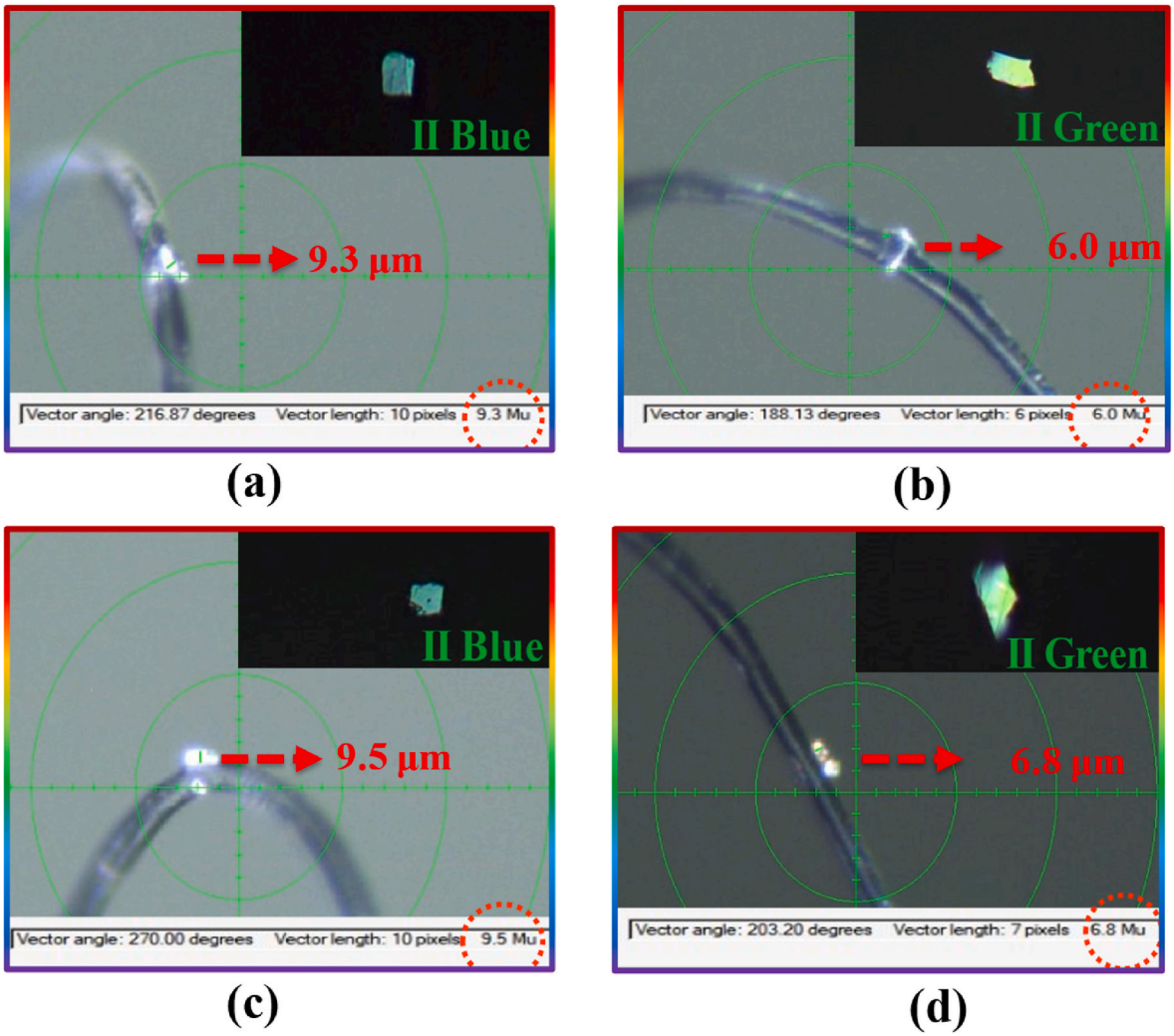

Fig. 4. The photographs of crystal size and their interference colors observed in the cross-polarized light for (a) $BaGe_2O_4S$ (b) $BaGe_2O_4Se$ (c) $SrGe_2O_4S$ and (d) $SrGe_2O_4Se$.

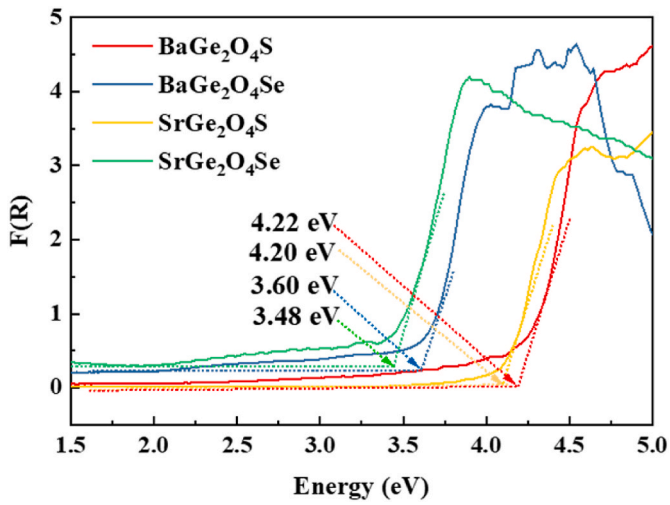

Fig. 5. UV–vis–NIR optical absorption spectra of AGe_2O_4Q (A = Ba, Sr; Q = S, Se).

eV and 3.48 eV, respectively, which are larger than singe-anionic classical chalcogenide compounds, such as $AgGaS_2$ (2.56 eV) [46], $AgGaSe_2$ (1.83 eV) [47], and can be comparable to some oxide-based crystals, such as $Sr_2CdGe_2O_7$ (2.89 eV) [48], $NaCa_4V_5O_{17}$ (2.74 eV) [49], $Li_2K_4TiOGe_4O_{12}$ (4.43 eV) [50], etc. Meanwhile, in order to evaluate the IR transmission of AGe_2O_4Q (A = Ba, Sr; Q = S, Se), their IR spectra were also measured (Fig. S2). That shows that there are no distinct absorption peaks existing in the range from 4000 to 1050 cm^{-1}, corresponding to wide transmission range from 2.5 μm to 9.5 μm. Therefore, AGe_2O_4Q (A = Ba, Sr; Q = S, Se) would be potential as mid-IR optical materials. Then, there are three absorption peaks (≈1050, 700 and 500 cm^{-1}) observed in their respective IR spectra, which can be attributed to the Ge–O and Ge–S/Se stretching mode [51,52]. All of these assignments are consistent with those of other compounds containing Ge–S/Se and Ge–O groups, such as GeO_2 [53], GeS_2 [54], $Ae_3Q[GeOQ_3]$ (Ae = Ba, Sr; Q = S, Se) [51], etc.

3.5. Raman spectroscopy

To deeply analyze the specific absorption spectra of different units, the Raman spectra of AGe_2O_4Q (A = Ba, Sr; Q = S, Se) were measured using the micron-sized crystals. As shown in Fig. S3, the strong absorption peaks in the range of 874−472 cm^{-1} can be attributed to the characteristic vibrations of the Ge−O−Ge bonds, while the peaks in the range of 377−260 cm^{-1} are for the Ge−S/Se bonds. The appearance of these vibrational peaks also shows that there are Ge–O or Ge–S/Se bonds in the compounds of AGe_2O_4Q (A = Ba, Sr; Q = S, Se). Besides, these absorption peaks below 200 cm^{-1} might be related to the vibrations of Ba/Sr–S or Ba/Sr–Se bonds, respectively [55–57].

3.6. Theoretical calculations

The electronic band structures of AGe_2O_4Q (A = Ba, Sr; Q = S, Se) were calculated by the DFT as shown in Fig. S4. For AGe_2O_4Q (A = Ba, Sr; Q = S, Se), the top of the valence band (VB) and the bottom of the conduction band (CB) are located at the same G-point, describing the

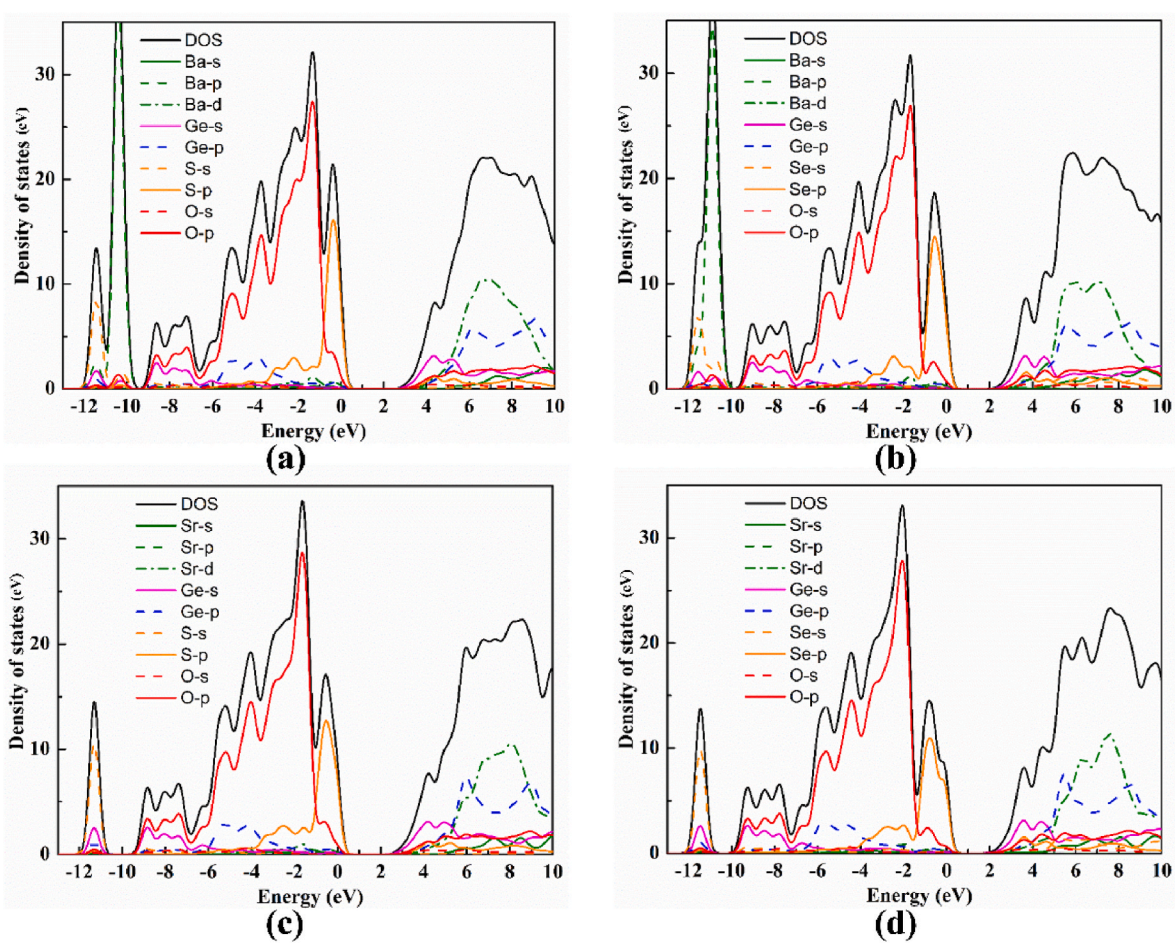

Fig. 6. Calculated total and partial DOS for (a) $BaGe_2O_4S$, (b) $BaGe_2O_4Se$, (c) $SrGe_2O_4S$, and (d) $SrGe_2O_4Se$.

indirect bandgaps of 2.83 eV for $BaGe_2O_4S$, 2.33 eV for $BaGe_2O_4Se$, 2.60 eV for $SrGe_2O_4S$ and 2.13 eV for $SrGe_2O_4Se$, respectively. Clearly, these band-gaps are underestimated by the GGA as the exchange–correlation functional [40]. Four compounds also exhibit the similar density of states (DOS) and partial density of states (PDOS) (Fig. 6). The Ge *4s*,*4p*, S/Se *3p*, and O *2p* orbitals construct the top region of valence states from −9.6 to 0 eV. Their wide hybridization in this area indicates that Ge–O and Ge–S/Se bonds make the main contribution of the upper side of the valence band. The bottom region of conduction states mainly is composed of *4s*, *4p* states of Ge, *3p* state of S/Se, and *2p* state of O. Thus, [GeO_3S/Se] and [GeO_4] tetrahedra have the significant effect on its optical properties, which determine the birefringent of AGe_2O_4Q (A = Ba, Sr; Q = S, Se).

The refractive indices of AGe_2O_4Q (A = Ba, Sr; Q = S, Se) and $BaGe_2O_5$ were also calculated by DFT. As shown in Fig. 7, the calculated birefringence values for $BaGe_2O_4S$, $BaGe_2O_4Se$, $SrGe_2O_4S$ and $SrGe_2O_4Se$ at 1064 nm are 0.13, 0.16, 0.15 and 0.19, respectively, while the birefringence of $BaGe_2O_5$ is only 0.03 at 1064 nm. Therefore, it is clear that the birefringence of compounds is indeed largely enhanced from single-anionic compounds to heteroanionic compounds. The birefringence values of AGe_2O_4Q (A = Ba, Sr; Q = S, Se) are comparable to those of the commercialized birefringent crystals, such as α-BaB_2O_4 (Δn = 0.116 at 1064 nm) [58], YVO_4 (Δn = 0.225 at 1064 nm) [7] and $CaCO_3$ (Δn = 0.171 at 633 nm) [10]. So, they are potentials as IR birefringent crystals.

3.7. The dipole moment calculations

As is well known, the anisotropic polarization of the structure is the main cause of material birefringence [59]. Due to the fact that alkaline cations typically exhibit spherically symmetric coordination, their contribution to birefringence can be negligible. The birefringence is mainly determined by the highly asymmetric anion groups [60]. In order to further understand the relationship between the structure and birefringence, the anisotropy of anion groups can be quantified by calculating their dipole moments. As described above, the dipole moments of the anion groups, the [GeO_6] polyhedra and [GeO_4] tetrahedra in $BaGe_2O_5$, and the [GeO_4] and [GeO_3Q] tetrahedra in $BaGe_2O_4Q$, are calculated according to the bond valences method [42]. As shown in Table 2, the dipole moments from the [GeO_6] polyhedra and [GeO_4] tetrahedra in $BaGe_2O_5$ are very small (μ = 2.99 and 0.44 Debye (D), respectively). However, in $BaGe_2O_4Q$, the heteroanions [GeO_3Q] (Q = S, Se) and [GeO_4] units have larger dipole moments, 5.5–14.11 D and 4.16–4.76 D, respectively. Generally, the larger dipole moments can generate the larger birefringence [61–63]. Therefore, the calculations of dipole moments are also consistent with their birefringence magnitudes.

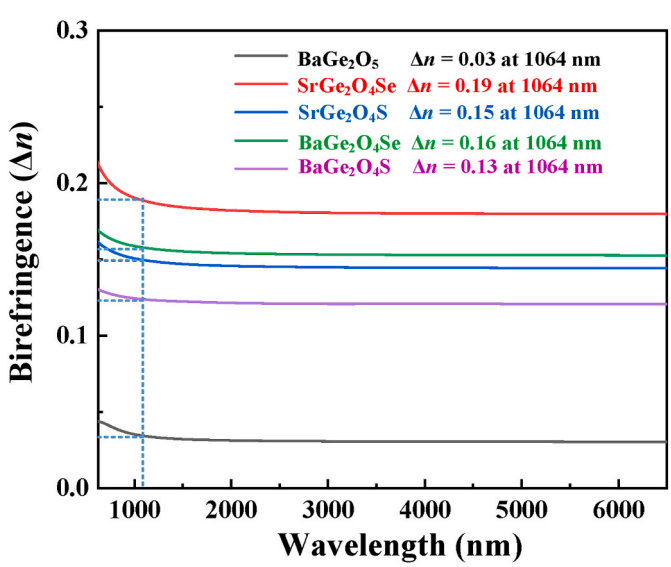

Fig. 7. Dispersion of birefringence (Δn) of $BaGe_2O_4S$, $BaGe_2O_4Se$, $SrGe_2O_4S$, $SrGe_2O_4Se$ and $BaGe_2O_5$.

Table 2
Comparison of dipole moments for GeO_3S/Se mixed-anion units and GeO_4 and GeO_6 single-anionic units.

Compounds	Polyhedra	Magnitude (D)	Δn (at 1064 nm)
$BaGe_2O_5$	GeO_6	2.99	0.03
	GeO_4	0.44	
$BaGe_2O_4S$	GeO_3S	7.25	0.13
	GeO_4	4.16	
$BaGe_2O_4Se$	GeO_3Se	14.11	0.16
	GeO_4	4.64	
$SrGe_2O_4S$	GeO_3S	5.50	0.15
	GeO_4	4.58	
$SrGe_2O_4Se$	GeO_3Se	11.32	0.19
	GeO_4	4.76	

4. Conclusion

In summary, four new heteroanionic oxychalcogenides, AGe_2O_4Q (A = Ba, Sr; Q = S, Se), have been synthesized by the solid-state reaction. They all contain 2D heteroanionic [Ge_2O_4Q] layers. Compared with the single-anionic $BaGe_2O_5$, the octahedral [GeO_6] units are changed to tetrahedral [GeO_3Q] units. And owing to the larger polarization anisotropy of [GeO_4] and [GeO_3Q] units, AGe_2O_4Q (A = Ba, Sr; Q = S, Se) all exhibit relatively large birefringence, 0.13, 0.16, 0.15 and 0.19 at 1064 nm, for $BaGe_2O_4S$, $BaGe_2O_4Se$, $SrGe_2O_4S$ and $SrGe_2O_4Se$ respectively. These birefringence values are one-order magnitude larger than their single-anionic germanate, $BaGe_2O_5$ (0.03 @ 1064 nm). It indicates that constructing heteroanionic oxychalcogenides is a feasible strategy for enhancing the birefringence of materials. In addition, AGe_2O_4Q (A = Ba, Sr; Q = S, Se) all exhibit large E_g (3.48–4.32 eV) and wide the IR transparent region (2.5–9.5 μm). Therefore, AGe_2O_4Q (A = Ba, Sr; Q = S, Se) may be potential as IR birefringent crystals.

Accession codes

CCDC 2279313–2279316 contain the supplementary crystallographic data for this paper. These data can be obtained free of charge via www.ccdc.cam.ac.uk/data_request/cif, or by emailing data_request@ccdc.cam.ac.uk, or by contacting The Cambridge Crystallographic Data Centre, 12 Union Road, Cambridge CB2 1EZ, UK; fax: +44 1223 336033.

CRediT authorship contribution statement

Dong Gao: Conceptualization, Methodology, Writing - original draft, preparation. **Fuqiang Chen:** Data curation, Investigation. **Hongping Wu:** Formal analysis. **Zhanggui Hu:** Project administration. **Jiyang Wang:** Validation. **Yicheng Wu:** Funding acquisition. **Hongwei Yu:** Supervision. **P Shiv Halasyamani:** Writing - review & editing.

Declaration of competing interest

The authors declare that they have no known competing financial interests or personal relationships that could have appeared to influence the work reported in this paper.

Data availability

Data will be made available on request.

Acknowledgements

This work is supported by the National Natural Science Foundation of China (Grant Nos. 52172006, 52322202, 22071179, 51972230, 51890864 and 51890865), the Natural Science Foundation of Tianjin (Grant Nos. 20JCJQJC00060 and 21JCJQJC00090). PSH thanks the Welch Foundation (Grant E-1457) and the NSF (DMR-2002319) for support.

Supporting information

Atomic coordinates, equivalent isotropic displacement parameters, bond valence sum, table of bond lengths and angles, the IR and Raman spectra for AGe_2O_4Q (A = Ba, Sr; Q = S, Se) and calculated band structures.

Appendix A. Supplementary data

Supplementary data to this article can be found online at.

References

[1] A. Tudi, S. Han, Z. Yang, S. Pan, Potential optical functional crystals with large birefringence: recent advances and future prospects, Coord. Chem. Rev. 459 (2022), e214380.
[2] Y. Chu, K. Wu, X. Su, J. Han, Z. Yang, S. Pan, Intriguing structural transition inducing variable birefringences in ABa_2MS_4Cl (A = Rb, Cs; M = Ge, Sn), Inorg. Chem. 57 (2018), 11310.
[3] R. Wang, F. Liang, X. Liu, Y. Xiao, Q. Liu, X. Zhang, L.M. Wu, L. Chen, F. Huang, Heteroanionic melilite oxysulfide: a promising infrared nonlinear optical candidate with a strong second-harmonic generation response, sufficient birefringence, and wide bandgap, ACS Appl. Mater. Interfaces 14 (2022), 23645.
[4] A. Abudurusuli, K. Wu, A. Tudi, Z. Yang, S. Pan, $ABaSbQ_3$ (A = Li, Na; Q = S, Se): Diverse arrangement modes of isolated SbQ_3 ligands regulating the magnitudes of birefringences, Chem. Commun. 55 (2019) 5143.
[5] X. Ji, H. Wu, B. Zhang, H. Yu, Z. Hu, J. Wang, Y. Wu, Intriguing dimensional transition inducing variable birefringence in $K_2Na_2Sn_3S_8$ and $Rb_3NaSn_3Se_8$, Inorg. Chem. 60 (2021) 1055.
[6] L.J. Yao, C.L. Hu, Z. Fang, J.G. Mao, $Hg_2P_2S_6$: a layered mercury hexathiodiphosphate (IV) with large birefringence, J. Solid State Chem. 315 (2022), e123433.
[7] H.T. Luo, T. Tkaczyk, E.L. Dereniak, K. Oka, R. Sampson, High birefringence of the yttrium vanadate crystal in the middle wavelength infrared, Opt. Lett. 31 (2006) 616.
[8] J.R. Devore, Refractive indices of rutile and sphalerite, J. Opt. Soc. Am. 41 (1951) 416.
[9] R.V. Schmidt, I.P. Kaminow, Metal-diffused optical waveguides in $LiNbO_3$, Appl. Phys. Lett. 25 (1974) 458.
[10] D. Achlioptas, R.M. D'Souza, J. Spencer, Explosive percolation in random networks, Sci 323 (2009) 1453.
[11] H. Zhang, M. Zhang, S. Pan, Z. Yang, Z. Wang, Q. Bian, X. Hou, H. Yu, F. Zhang, K. Wu, F. Yang, Q. Peng, Z. Xu, K.B. Chang, K.R. Poeppelmeier, $Na_3Ba_2(B_3O_6)_2F$: next generation of deep-ultraviolet birefringent materials, Cryst. Growth Des. 15 (2015) 523.
[12] Z. Jia, N. Zhang, Y. Ma, L. Zhao, M. Xia, R. Li, Top-seeded solution growth and optical properties of deep-UV birefringent crystal $Ba_2Ca(B_3O_6)_2$, Cryst. Growth Des. 17 (2017) 558.
[13] X.S. Lv, Y.L. Sun, J. Han, G.X. Gu, S.M. Wan, M.J. Cheng, S.L. Pan, Q.L. Zhang, Growth and Raman spectrum of $Ba_2Mg(B_3O_6)_2$ crystal, J. Cryst. Growth 363 (2013) 220.
[14] X. Chen, F. Zhang, Y. Shi, Y. Sun, Z. Yang, S. Pan, $MBaYB_6O_{12}$ (M = Rb, Cs): two new rare-earth borates with large birefringence and short ultraviolet cutoff edges, Dalton Trans. 47 (2018) 750.
[15] N.G. Margiani, G.A. Mumladze, I.G. Kvartskhava, A.S. Kuzanyan, G.R. Badalyan, V. V. Zhghamadze, Impact of $Ca(BO_2)_2$ Doping on high-TcPhase formation and transport properties of Bi(Pb)-2223 superconductor, IEEE Trans. Appl. Supercond. 32 (2022), e3146817.
[16] S. Han, A. Tudi, W. Zhang, X. Hou, Z. Yang, S. Pan, Recent development of Sn(II), Sb(III)-based birefringent material: crystal chemistry and investigation of birefringence, Angew. Chem. Int. Ed. 62 (2023), e202302025.
[17] Y. Li, X. Zhang, Y. Zhou, W. Huang, Y. Song, H. Wang, M. Li, M. Hong, J. Luo, S. Zhao, An optically anisotropic crystal with large birefringence arising from cooperative π orbitals, Angew. Chem. Int. Ed. 61 (2022), e202208811.
[18] L. Zhu, M. Gai, W. Jin, Y. Yang, Z. Yang, S. Pan, Barium fluoroiodate crystals with a large band gap and birefringence, Inorg. Chem. Front. 8 (2021) 3127.
[19] J. Yao, D. Mei, L. Bai, Z. Lin, W. Yin, P. Fu, Y. Wu, $Baga_4Se_7$: a new congruent-melting IR nonlinear optical material, Inorg. Chem. 49 (2010) 9212.
[20] Z.Z. Luo, C.S. Lin, W.L. Zhang, H. Zhang, Z.Z. He, W.D. Cheng, $Ba_{18}F_{18}In_8S_{21}$ and $Ba_9F_{10}In_4S_{10}$: new kind of mixed anion compounds with the novel low-dimensional structure, CrystEngComm 16 (2014) 2788.
[21] G. mao Li, Q. Liu, K. Wu, Z. hua Yang, S. lie Pan, $Na_2CdGe_2Q_6$ (Q = S, Se): two metal-mixed chalcogenides with phase-matching abilities and large second-harmonic generation responses, Dalton Trans. 46 (2017) 2778.
[22] Z. Li, Y. Liu, S. Zhang, W. Xing, W. Yin, Z. Lin, J. Yao, Y. Wu, Functional chalcogenide $Na_2HgSn_2Se_6$ and $K_2MnGe_2Se_6$ exhibiting flexible chain structure and intriguing birefringence tunability, Inorg. Chem. 59 (2020) 7614.
[23] Y. Song, S. Cui, Z. Qian, H. Yu, Z. Hu, J. Wang, Y. Wu, H. Wu, $[ASr_4Cl][Ge_3S_{10}]$ (A = Na, K) and $[KBa_4Cl][Ge_3S_{10}]$: new salt-inclusion infrared nonlinear optical crystals with zero-dimensional $[Ge_3S_9]$ clusters, Inorg. Chem. Front. 9 (2022) 5932.
[24] K. Wu, S. Pan, Z. Yang, Ba_2GeS_4 and Mg_2SnS_4: synthesis, structures, optical properties and electronic structures, RSC Adv. 5 (2015), 33646.
[25] W. Xing, P. Fang, N. Wang, Z. Li, Z. Lin, J. Yao, W. Yin, B. Kang, Two mixed-anion units of $[GeOSe_3]$ and $[GeO_3S]$ originating from partial isovalent anion substitution and inducing moderate second harmonic generation response and large birefringence, Inorg. Chem. 59 (2020), 16716.
[26] L. Jiang, L. Han, C. Lu, S. Yang, Y. Liu, H. Jiang, Y. Yan, X. Tang, D. Yang, Cu_2Se as textured adjuvant for Pb-doped BiCuSeO materials leading to high thermoelectric performance, ACS Appl. Mater. Interfaces 13 (2021), 11977.
[27] E.M. Sorensen, H.K. Izumi, J.T. Vaughey, C.L. Stern, K.R. Poeppelmeier, $Ag_4V_2O_6F_2$: an electrochemically active and high silver density phase, J. Am. Chem. Soc. 127 (2005) 6347.
[28] L.T. Menezes, E. Gage, A. Assoud, M. Liang, P.S. Halasyamani, H. Kleinke, $Sr_6Ge_3OSe_{11}$: a rationally designed noncentrosymmetric oxyselenide with polar $[GeOSe_3]$ building blocks, Chem. Mater. 35 (2023) 3033.
[29] X. Zhang, J. Zhang, J. Xu, Q. Su, Luminescent properties of Eu^{2+}-activated $SrLaGa_3S_6O$ phosphor, J. Alloys Compd. 389 (2005) 247.
[30] Y. Zhang, H. Wu, Z. Hu, J. Wang, Y. Wu, H. Yu, Achieving strong second harmonic generation response and wide band gap in a Hg-based material, Inorg. Chem. Front. 16 (2022) 4075.
[31] J.N. Li, X.H. Li, Y.X. Xu, W.L. Liu, S.P. Guo, First investigation of nonlinear optical oxychalcogenide with three-dimensional anionic Framework and special Windmill-Like functional Motifs, Chin, J. Chem. 40 (2022) 2407.
[32] N. Zhang, X. Huang, W.D. Yao, Y. Chen, Z.R. Pan, B.X. Li, W.L. Liu, S.P. Guo, $Eu_2MGe_2OS_6$ (M = Mn, Fe, Co): three melilite-type rare-earth Oxythiogermanates exhibiting balanced nonlinear-optical Behaviors, Inorg. Chem. 62 (2023), 16299.
[33] A. Nakatsuka, K. Sugiyama, M. Ohkawa, O. Ohtaka, K. Fujiwara, A. Yoshiasa, A new high-pressure strontium germanate, $SrGe_2O_5$, Acta. Crystallogr C. Struct. Chem. 72 (2016) 716.
[34] G.M. Sheldrick, Shelxt - Integrated space-group and crystal-structure determination, Acta Crystallogr. A. 71 (2015) 3.
[35] K. Mohana Priyadarshini, A. Chandramohan, T. Uma Devi, Synthesis, growth, crystal structure and characterization of the o-toluidinium picrate, J. Cryst. Process Technol. 3 (2013) 123.
[36] A.L. Spek, Single-crystal structure validation with the Program PLATON, J. Appl. Crystallogr. 36 (2003) 7.
[37] V. Milman, K. Refson, S.J. Clark, C.J. Pickard, J.R. Yates, S.P. Gao, P.J. Hasnip, M.I. J. Probert, A. Perlov, M.D. Segall, Electron and vibrational spectroscopies using DFT, plane waves and pseudopotentials: CASTEP implementation, J. Mol. Struct.: THEOCHEM 954 (2010) 22.
[38] S.J. Clark, M.D. Segall, C.J. Pickard Ii, P.J. Hasnip, M.I.J. Probert, K. Refson, M. C. Payne, First principles methods using CASTEP, Z. für KristallographieCrystline, Mater. 220 (2005) 567.
[39] A.M. Rappe, K.M. Rabe, E. Kaxiras, J.D. Joannopoulos, Optimized pseudopotentials, Phys. Rev. B Condens. Matter 41 (1990) 1227.
[40] J.P. Perdew, S. Kurth, A. Zupan, P. Blaha, Accurate density functional with correct formal properties: a step beyond the generalized gradient approximation, Phys. Rev. Lett. 82 (1999) 2544.
[41] M.Y. Ran, S.H. Zhou, B. Li, W. Wei, X.T. Wu, H. Lin, Q.L. Zhu, Enhanced second-harmonic-generation efficiency and birefringence in melillite oxychalcogenides $Sr_2MGe_2OS_6$ (M = Mn, Zn, and Cd), Chem. Mater. 34 (2022) 3853.
[42] H. Di Yang, S.H. Zhou, M.Y. Ran, X.T. Wu, H. Lin, Q.L. Zhu, Melilite oxychalcogenide $Sr_2FeGe_2OS_6$: a phase-matching IR nonlinear optical material realized by isomorphous substitution, Inorg. Chem. Front. 10 (2023) 2030.
[43] I. Brown, D. Altermatt, Bond-valence parameters obtained from a systematic analysis of the Inorganic crystal structure Database, Acta Crystallogr. 41 (2010) 244.
[44] P.E. Blochl, Projector augmented-wave method, Phys. Rev. B Condens. Matter 50 (1994), 17953.
[45] J. Tauc, Absorption edge and internal electric fields in amorphous semiconductors, Mater. Res. Bull. 5 (1970) 721.
[46] H.M. Zhou, L. Xiong, L. Chen, L.M. Wu, Dislocations that decrease size mismatch within the lattice leading to ultrawide band gap, large second-order susceptibility, and high nonlinear optical performance of $AgGaS_2$, Angew. Chem. Int. Ed. 58 (2019) 9979.
[47] J.K. Larsen, O. Donzel-Gargand, K.V. Sopiha, J. Keller, K. Lindgren, C. Platzer-Bjorkman, M. Edoff, Investigation of $AgGaSe_2$ as a wide gap solar cell absorber, ACS Appl. Energy Mater. 4 (2021) 1805.
[48] P. Becker, P. Held, J. Liebertz, L. Bohatý, Optical properties of the germanate melilites $Sr_2MgGe_2O_7$, $Sr_2ZnGe_2O_7$ and $Ba_2ZnGe_2O_7$, Cryst. Res. Technol. 44 (2009) 603.
[49] Z. Xie, S. Cheng, S. Li, H. Ding, $NaCa_4V_5O_{17}$ with isolated V_2O_7 dimer and V_3O_{10} trimer exhibiting a large birefringence, J. Solid State Chem. 269 (2019) 94.

[50] J. Xu, H. Wu, H. Yu, W. Zhang, Z. Hu, J. Wang, Y. Wu, P.S. Halasyamani, $Li_2K_4TiOGe_4O_{12}$: a stable mid-infrared nonlinear optical material, Chem. Mater. 32 (2020) 906.
[51] S. Cui, H. Wu, Z. Hu, J. Wang, Y. Wu, H. Yu, The antiperovskite-type oxychalcogenides $Ae_3Q[GeOQ_3]$ (Ae = Ba, Sr; Q = S, Se) with large second harmonic generation responses and wide band gaps, Adv. Sci. 10 (2023), 202204755.
[52] H. Liu, Z. Song, H. Wu, Z. Hu, J. Wang, Y. Wu, H. Yu, $[Ge_2O_3S_2]$: an unprecedented heteroanionic infrared nonlinear optical material containing three typical anions, ACS Mater. Lett. 4 (2022) 1593.
[53] Q.J. Liu, Z.T. Liu, L.P. Feng, H. Tian, First-principles study of structural, elastic, electronic and optical properties of rutile GeO_2 and α-quartz GeO_2, Solid State Sci. 12 (2010) 1748.
[54] J. Málek, J. Chovanec, R. Svoboda, Y. Taniguchi, H. Kawaji, Heat capacity of vitreous GeS_2, J. Chem. Thermodyn. 81 (2015) 101.
[55] R. Wang, F. Liang, F. Wang, Y. Guo, X. Zhang, Y. Xiao, K. Bu, Z. Lin, J. Yao, T. Zhai, F. Huang, $Sr_6Cd_2Sb_6O_7S_{10}$: strong SHG response activated by highly polarizable Sb/O/S groups, Angew. Chem. Int. Ed. 58 (2019) 8078.
[56] N. Zhang, Q.T. Xu, Z.H. Shi, M. Yang, S.P. Guo, Characterizations and nonlinear-optical properties of pentanary transition-metal oxysulfide $Sr_2CoGe_2OS_6$, Inorg. Chem. 61 (2022), 17002.
[57] Y. Yun, W. Xie, Y. Huang, Z. Yang, K. Wu, G. Li, S. Pan, $NaBaBS_3$: a promising infrared functional material with large birefringence induced by π-conjugated $[BS_3]$ units, Chem. Mater. 34 (2022) 5215.
[58] Y. Zhang, Q. Bian, H. Wu, H. Yu, Z. Hu, J. Wang, Y. Wu, Designing a new infrared nonlinear optical material, β-$Baga_2Se_4$ inspired by the phase transition of the BaB_2O_4 (BBO) crystal, Angew. Chem. Int. Ed. 61 (2022), e202115374.
[59] D. Gao, X. Ji, H. Yu, Z. Hu, J. Wang, Y. Wu, H. Wu, Syntheses, structures, and characterization of new heteroanionic chalcohalides: $Na_2Ba_{17}In_8Q_{21}F_{18}$ (Q = S, Se), $KBa_2InQ_3F_2$ (Q = S, Se), J. Alloys, Compd 936 (2023), e148141.
[60] X. Tian, X. Zhang, Y. Xiao, X. Wu, B. Zhang, D. Yang, K. Wu, From oxides to oxysulfides: the mixed-anion GeS_3O unit induces huge improvement in the nonlinear optical effect and optical anisotropy for potential nonlinear optical materials, RSC Adv. 12 (2022), 16296.
[61] H. Yu, W. Zhang, P.S. Halasyamani, Large Birefringent Materials, $Na_6Te_4W_6O_{29}$ and $Na_2TeW_2O_9$: synthesis, structure, crystal growth, and characterization, Cryst. Growth Des. 16 (2016) 1081.
[62] L. Wang, C. Tu, H. Gao, J. Zhou, H. Wang, Z. Yang, S. Pan, J. Li, Clamping effect driven design and fabrication of new infrared birefringent materials with large optical anisotropy, Sci. China Chem. 66 (2023) 1086.
[63] C. Jin, F. Li, Z. Yang, S. Pan, M. Mutailipu, $[C_3N_6H_7]_2[B_3O_3F_4(OH)]$: a new hybrid birefringent crystal with strong optical anisotropy induced by mixed functional units, J. Mater. Chem. C 10 (2022) 6590.